

19 **Abstract.** A popular way to forecast streamflow is to use bias-corrected
20 meteorological forecast to drive a calibrated hydrological model, but these
21 hydrometeorological approaches have deficiency over small catchments due to
22 uncertainty in meteorological forecasts and errors from hydrological models,
23 especially over catchments that are regulated by dams and reservoirs. For a cascade
24 reservoir catchment, the discharge of the upstream reservoir contributes to an
25 important part of the streamflow over the downstream areas, which makes it
26 tremendously hard to explore the added value of meteorological forecasts. Here, we
27 integrate the meteorological forecast, land surface hydrological model simulation and
28 machine learning to forecast hourly streamflow over the Yantan catchment, where the
29 streamflow is influenced both by the upstream reservoir water release and the
30 rainfall-runoff processes within the catchment. Evaluation of the hourly streamflow
31 hindcasts during the rainy seasons of 2013-2017 shows that the hydrometeorological
32 ensemble forecast approach reduces probabilistic and deterministic forecast errors by
33 6% as compared with the traditional ensemble streamflow prediction (ESP) approach
34 during the first 7 days. The deterministic forecast error can be further reduced by 6%
35 in the first 72 hours when combining the hydrometeorological forecast with the long
36 short-term memory (LSTM) deep learning method. However, the forecast skill for
37 LSTM using only historical observations drops sharply after the first 24 hours. This
38 study implies the potential of improving flood forecast over a cascade reservoir
39 catchment by integrating meteorological forecast, hydrological modeling and machine
40 learning.

41 **Keywords:** Streamflow; Hydrological modeling; LSTM; Reservoir; Ensemble

42 forecast

43

44 **1. Introduction**

45 Flood events are the most destructive ones among the natural disasters, causing
46 huge damages to human society. Reservoirs are massively constructed to regulate
47 river flows, which has significantly reduced flood risks or damages (Ji et al., 2020).
48 However, the number and intensity of precipitation extreme events are increasing in
49 many areas as the global warming continues, thus amplify the potential of flood
50 hazards (Hao et al., 2013; Shao et al., 2016; Wei et al., 2018; Yuan et al., 2018a;
51 Wang et al., 2019). Accurate streamflow forecast is thus needed to provide guidelines
52 for reservoir operations (Robertson et al., 2013), especially when the flood risk is
53 increasing under global warming.

54 A common approach of streamflow forecast is to use hydrological models, where
55 the first attempt could be traced back to 1850s, using simple regression-type
56 approaches to predict discharge from observed precipitation (Mulvaney, 1850). Since
57 then, model concepts have been further augmented by designing new data networks,
58 addressing heterogeneity of hydrological processes, capturing the nonlinear
59 characteristics of hydrologic system and parameterizing models (Hornberger and
60 Boyer, 1995; Kirchner, 2006). With the advancements of computer technology and
61 high-resolution observation, a well-parameterized hydrological model can simulate
62 streamflow with high accuracy (Kollet et al., 2010; Ye et al., 2014; Graaf et al., 2015;
63 Yuan et al., 2018b).

64 Streamflow simulations from hydrological models heavily rely on
65 meteorological forcing inputs, especially precipitation, which can be measured at
66 in-situ gauges or retrieved from satellites and radars. However, for medium-range (2–
67 15 days ahead) streamflow forecasts, precipitation forecast is needed (Hopson et al.,
68 2002). To improve the forecast, ensemble techniques that can give a deterministic
69 estimate as well as its uncertainty became popular. Ensemble weather forecasting can
70 be traced back to 1963 when Leith transferred a deterministic forecast into an
71 ensemble using the Monte-Carlo method to describe the atmospheric uncertainty
72 (Leith, 1963). In the 1990s, ensemble forecasting was developed into an integral part
73 of numerical weather prediction, which showed higher skill than the deterministic
74 forecast even with higher model resolution (Toth et al., 2001). Due to its rapid
75 development, ensemble weather forecasts and climate predictions are applied to
76 hydrological forecasting studies by combining with hydrological models (Jasper et al.,
77 2002; Balint et al., 2006; Jaun et al., 2008; Xu et al., 2015; Yuan et al., 2016; Zhu et
78 al., 2019). Provided with streamflow variability, a reservoir can maintain a reliable
79 utility from natural streamflow better than provided with a deterministic streamflow
80 forecast (Zhao et al., 2011). However, the streamflow prediction skill depends on
81 whether the precipitation forecasts introduced into the hydrological model are skillful
82 (Alfieri et al., 2013). When assessing the skill of this hydrometeorological forecast
83 approach, a benchmark is needed. Using ensembles of historical climatology data
84 (Day, 1985) as meteorological forecast inputs, which is known as ensemble
85 streamflow prediction (ESP), is often selected as the benchmark approach.

86 Evaluations of hydrological forecasts indicated that forecast skill has a close
87 relationship with catchment size, geographical locations and resolutions (Alfieri et al.,
88 2013; Pappenberger et al., 2015), which means there is a necessity to compare with
89 the ESP to show the skill of the hydrometeorological forecast approach.

90 Although physically based hydrological models are widely used, it is still hard
91 to apply a hyper-resolution distributed model for streamflow forecasting due to its
92 demand for observation data, complex model structures and computational resources
93 requirements for calibration and application (Wood et al., 2011; Kratzert et al., 2018;
94 Yaseen et al., 2018). In cascade reservoir systems, there are two sources of streamflow,
95 one is from the rainfall within the interval basin and the other is from the upstream
96 reservoir discharge. While the rainfall-runoff relationship is well studied, it is
97 challenging to reproduce the reservoir operating rules in a physical model (Gao et al.,
98 2010; Zhang et al., 2016; Dang et al., 2020).

99 Machine learning methods can recognize patterns hidden in input data and can
100 simulate or predict streamflow without explicit descriptions of the underlying physical
101 processes (Kisi et al., 2007; Adnan et al., 2019). Neural networks are suitable for
102 streamflow forecasting among machine learning models, some of them can even
103 outperform physically based hydrological models. For example, Humphrey et al.
104 (2016) showed that their combined Bayesian artificial neural network with the mod è
105 du Génie Rural à 4 paramètres Journalier (GR4J) approach outperforms the GR4J
106 model in monthly streamflow forecasting. Kratzert et al. (2019) showed that the long

107 short-term memory (LSTM)-based approach outperforms a well-calibrated
108 Sacramento Soil Moisture Accounting Model (SAC-SMA). Yang et al. (2020) used
109 the geomorphology-based hydrological model (GBHM) combined with traditional
110 ANN model to simulate daily streamflow, which can provide enough physical
111 evidence and can run with less observation data. Although neural network models are
112 criticized with little physical evidence (Abrahart et al., 2012), their potential in
113 hydrological forecasting is yet to be explored.

114 In this study, we combine the machine learning with hydrometeorological
115 approach for hourly streamflow forecast over a cascade reservoir catchment located in
116 southwestern China. We use the meteorological hindcast data from European Centre
117 for Medium-Range Weather Forecasts (ECMWF) model that participated in the
118 THORPEX Interactive Grand Global Ensemble (TIGGE) project to drive a newly
119 developed high-resolution land surface model, named as the Conjunctive
120 Surface-Subsurface Process model version 2 (CSSPv2, Yuan et al., 2018b), to provide
121 runoff and streamflow forecasts, and correct the forecasts via LSTM model. We aim
122 to improve flood forecast over the cascade reservoir catchment by integrating
123 meteorological forecast, hydrological modeling and machine learning. So we strive to
124 (1) calibrate the hydrological model, (2) bias correct the meteorological forecasts, (3)
125 evaluate the streamflow forecast skill and (4) test the physical-statistical combined
126 approach.

127 **2. Study Area, Data, Model and Method**

128 *2.1 Study Area*

129 The Yantan Hydropower Station is in the middle reaches of Hongshui River in
130 Dahua Yao Autonomous County, Guangxi Province. The Yantan Hydropower Station
131 is the fifth level in the 10-level development of Hongshuihe hydropower base in
132 Nanpanjiang River, connected with upstream Longtan Hydropower Station and the
133 downstream Dahua Hydropower Station. The drainage area between the Longtan
134 Hydropower Station and Yantan Hydropower Station is 8,900 km². The annual mean
135 streamflow at Yantan gauge is 55.5 billion m³. The river passes through karst
136 mountain area, with narrow valley, steep slope and scattered cultivated land, and the
137 average slope is 0.036%. Figure 1 shows the locations of 4 hydrological gauges, with
138 detailed information listed in Table 1.

139 *2.2 Data and Method*

140 *2.2.1 Hydrometeorological observations*

141 There are 97 meteorological observation stations within the catchment (Figure
142 1). Here, observed hourly 2m-temperature, 10m-wind speed, relative humidity,
143 accumulated precipitation and surface pressure data were interpolated into a 5km
144 gridded observation dataset via inverse distance weight method. The hourly surface
145 downward solar radiation data from China Meteorological Administration Land Data
146 Assimilation System (CLDAS) was also interpolated into 5km via bilinear
147 interpolation method. The hourly surface downward thermal radiation was estimated

148 by specific humidity, pressure, temperature. This dataset was used to drive the
149 CSSPv2 land surface hydrological model.

150 The monthly runoff for each 5km grid was estimated by disaggregating control
151 streamflow station observations with the ratio of observed grid monthly precipitation
152 and catchment mean precipitation. The gridded runoff was used to calibrate the
153 CSSPv2 model at each grid (Yuan et al., 2016). The calibrated runoff parameters can
154 better represent the heterogeneity of the rainfall-runoff processes and make precise
155 runoff simulations.

156 *2.2.2 Ensemble Meteorological hindcast data and ESP hindcasts*

157 The TIGGE dataset consists of ensemble forecast data from 10 global Numerical
158 Weather Prediction centers started from October 2006, which has been made available
159 for scientific research, via data archive portals at ECMWF and the China
160 Meteorological Administration (CMA). TIGGE has become a focal point for a range
161 of research projects, including research on ensemble forecasting, predictability, and
162 the development of products to improve the prediction of severe weather (Bougeault
163 et al., 2010). In this paper, TIGGE data from April to September during 2013-2017
164 from ECMWF were used as meteorological hindcast data. The 3-hourly
165 meteorological hindcasts for 7-day lead time from 51 ensemble members (including
166 control forecast) were interpolated into 5km resolution via bilinear interpolation. The
167 forecast precipitation and temperature were corrected to match the observational
168 means to remove the biases.

169 The ESP was accomplished by applying historical meteorological forcings (Day,
170 1985). In this paper, the meteorological forcings from the same date as the forecast
171 start date to the next 9 days of each year (excluding the target year) were selected as
172 the ESP forcings. Take April 1st, 2013 as example, the 7-day observations started from
173 April 1st to April 10th (i.e., April 1st-April 7th, April 2nd-April 8th, ..., April 10th-April
174 16th) in the year of 2014, 2015, 2016 and 2017 were selected as the forecast ensemble
175 forcings of the issue date (April 1st), with a total of 40 ensemble members. The
176 detailed information about the raw datasets are listed in Table 2

177 2.2.3 CSSPv2 streamflow hindcasts

178 The physical hydrological model used in this paper is the Conjunctive
179 Surface-Subsurface Process model version 2 (CSSPv2; Yuan et al., 2018). The
180 CSSPv2 model is a distributed, grid-based land surface hydrological model, which
181 was developed from the Common Land Model (Dai et al., 2003, 2004), but with better
182 representations in lateral surface and subsurface hydrological processes and their
183 interactions. The routing model used here employs the kinetic wave equation as
184 covariance function, which is solved via a Newton algorithm. A main reason for
185 adopting this covariance function is that it suits the basin with mountainous terrain.
186 The CSSPv2 model was successfully used to perform a high-resolution (3 km) land
187 surface simulation over the Sanjiangyuan region, which is the headwater of major
188 Chinese rivers (Ji and Yuan, 2018). In this paper, we calibrated CSSPv2 model against
189 monthly estimated runoff to simulate the natural hydrological processes by using the

190 Shuffled Complex Evolution (SCE-UA) approach (Duan et al., 1994). The calibrated
 191 parameters include maximum velocity of baseflow, variable infiltration curve
 192 parameter, fraction of maximum soil moisture where non-linear baseflow occurs and
 193 fraction of maximum velocity of baseflow where non-linear baseflow begins. The
 194 hourly observed streamflow at Yantan hydrological gauge was used to calibrate the
 195 CSSPv2 routing model manually, including slope, river density, roughness, width and
 196 depth. The observed streamflow at Longtan hydrological gauge were added into the
 197 corresponding grid to provide upstream streamflow information. We used a
 198 high-resolution elevation database (hereafter referred to as DEM90) for sub-grid
 199 parameterization and figured out the initial values of these river channel parameters.
 200 We first extracted the slope angle and the natural river flow path from DEM90, and
 201 then identified the accurate river network using a drainage area threshold of 0.18 km².
 202 River density and bed slope values for each 5km grid were calculated as:

$$203 \quad \mathbf{rivden} = \sum \mathbf{l} / \mathbf{A}, \quad (1)$$

$$204 \quad \mathbf{bedslp} = \mathbf{mean}(\mathbf{tan}(\boldsymbol{\beta})), \quad (2)$$

205 where rivden is the river density (km/km²), bedslp is the river channel bed slope
 206 (unitless), A is the area of a 5km grid (km²), $\sum \mathbf{l}$ is the total river channel length (m)
 207 within the grid, $\boldsymbol{\beta}$ is the slope angle (radian) for each river segment located in the grid.

208 Other river channel parameters were estimated by empirical formulas (Getirana
 209 et al., 2012; Luo et al., 2017) as follows:

210
$$W = 1.956 \times A_{acc}^{0.413}, \quad (3)$$

211
$$H = 0.245 \times A_{acc}^{0.342}, \quad (4)$$

212
$$n = 0.03 + (0.05 - 0.03) \frac{H_{max} - H}{H_{max} - H_{min}}, \quad (5)$$

213 where W, H and n are river width (m), depth (m) and roughness (unitless) for each
214 5km grid; Aacc means the upstream drainage area (km²); Hmax and Hmin refer to the
215 maximum and minimum values of river depth calculated by Eq. (4).

216 Through a trial-and-error procedure, we calibrated these river channel parameters
217 to match the simulated streamflow with observed hourly records at Yantan
218 hydrological gauge. The simulation results were evaluated by calculating the
219 Nash-Sutcliffe efficiency (NSE) with corresponding observation data. The
220 descriptions of the calibrated parameters and their range are listed in Table 3

221 After calibration, we drove the CSSPv2 model using 5km regridded and
222 bias-corrected TIGGE-ECMWF forecast forcing during 2013-2017 to provide a set of
223 7-day hindcasts. Streamflow hindcasts both from the ESP and the hydrometeorological
224 approach (TIGGE-ECMWF/CSSPv2) were corrected by matching monthly mean
225 streamflow observations to remove the biases, and the hindcast experiments were
226 termed as ESP-Hydro and Meteo-Hydro (Table 4). Figure 2 shows the procession of
227 the CSSPv2 hindcasts: the calibrated CSSPv2 model was first driven with observation
228 dataset to generate initial hydrological conditions (soil moisture, surface water, etc.)
229 for each forecast issue date, then CSSPv2 model was driven with forecast data

230 (TIGGE-ECMWF or ESP) at every forecast issue date with the generated initial
231 conditions to perform a 7-day hindcast.

232 2.2.4 LSTM streamflow forecast

233 LSTM is a type of recurrent neural network model which learns from sequential
234 data. The input of the LSTM model includes forecast interval streamflow at the
235 specified forecast step obtained from TIGGE-ECMWF/CSSPv2, historical upstream
236 streamflow observation, and historical streamflow observation at Yantan hydrological
237 gauge. The network was trained on sequences of April to September in 2013-2017,
238 with six historical streamflow observations and one forecast interval streamflow to
239 predict the total streamflow at each forecast time step (Figure 2). The LSTM was
240 calibrated through a cross validation method, by leaving the target year out.

241 Before calibration, all input and output variables were normalized as follows:

$$242 \mathbf{q}_0 = \frac{(\mathbf{q} - \mathbf{q}_{\min})}{(\mathbf{q}_{\max} - \mathbf{q}_{\min})}, \quad (6)$$

243 Where \mathbf{q}_0 , \mathbf{q} , \mathbf{q}_{\max} and \mathbf{q}_{\min} are the normalized variable, input variable, the
244 maximum and minimum of the sequence of the variable, respectively. The hindcast
245 experiment was termed as Meteo-Hydro-LSTM (Table 2). In addition, we also tried
246 an LSTM streamflow forecast approach which only uses 6-hr historical streamflow
247 data as inputs, and the experiment was termed as LSTM (Table 2). The process of
248 LSTM is similar to Meteo-Hydro-LSTM but without the forecast interval streamflow,
249 which is also shown in Figure 2.

250 *2.3 Evaluation Method*

251 The root-mean squared error (RMSE) was used to evaluate the deterministic
252 forecast, i.e., the ensemble means of 51 (ECMWF) or 40 (ESP) forecast members. To
253 evaluate probabilistic forecasts, the Continuous Ranked Probability Score (CRPS)
254 was calculated as follows:

255
$$CRPS = \int_{-\infty}^{\infty} [F(\mathbf{y}) - F_o(\mathbf{y})]^2, \quad (7)$$

256 where

257
$$F_o(\mathbf{y}) = \begin{cases} \mathbf{0}, & \mathbf{y} < \mathbf{observed\ value} \\ \mathbf{1}, & \mathbf{y} \geq \mathbf{observed\ value} \end{cases} \quad (8)$$

258 is a cumulative-probability step function that jumps from 0 to 1 at the point where the
259 forecast variable \mathbf{y} equals the observation and $\mathbf{F}(\mathbf{y})$ is a cumulative-probability
260 distribution curve formed by the forecast ensembles. The CRPS has a negative
261 orientation (smaller values are better), and it rewards concentration of probability
262 around the step function located at the observed value (Wilks, 2005). The skill score
263 for deterministic forecast was calculated as

264
$$SS_{RMSE} = \frac{RMSE - RMSE_{ref}}{0 - RMSE_{ref}} = \mathbf{1} - \frac{RMSE}{RMSE_{ref}} \quad (9)$$

265 The skill score for probabilistic forecast (CRPSS) could be calculated similarly based
266 the CRPS.

267 **3. Results**

268 *3.1 Evaluation of CSSP calibration*

269 The employed CSSPv2 model is a fully distributed hydrological model and the
270 streamflow is calculated through a process of converting gridded rainfall into runoff
271 and a process of runoff routing. Figure 3 shows the runoff calibration results by
272 calculating the NSE of monthly runoff simulations compared with observed gridded
273 monthly runoff. After calibrating the CSSPv2 runoff model, the NSE of all grids are
274 above 0, which indicates that the runoff simulation results in all grids are more
275 reliable than the climatology method. In addition, grids distributed in the downstream
276 region have better NSE than the upstream grids. The NSE values of the grids in the
277 southern part are greater than 0.5, which accounts for two thirds of the interval basin
278 area. Higher NSE in the upstream part of Jiazhuan station (Figure 1) is due to more
279 humid climate (not shown), where hydrological models usually have better
280 performance over wetter areas. For the downstream areas with less precipitation, the
281 higher NSE is related to the higher percentage of sand in the soil (not shown). Under
282 the same meteorological conditions, there is higher hydraulic conductivity with higher
283 sand content (Wang et al., 2016), and it yields less runoff under infiltration excess,
284 which is more suitable for the saturation excess-based runoff generation for the
285 CSSPv2 model (Yuan et al., 2018b).

286 Figures 4 and 5 show the results after the calibration of the routing model, where
287 CSSPv2 is driven by observed meteorological forcings to provide streamflow
288 simulations and compare against observed streamflow at Yantan hydrological gauge.
289 Figure 4 shows the daily and monthly streamflow simulation results. The monthly
290 result (Fig. 4f) shows that the simulated streamflow closely follows the observed

291 streamflow, and the NSE is 0.96. The daily streamflow simulations during flood
292 seasons (Figs. 4a-4e) also show a good performance, and the NSE is 0.92. During
293 June and July in years of 2014, 2015 and 2017, the CSSPv2 model underestimated the
294 daily streamflow with a maximum of 1104 m³/s and an average of 334 m³/s (Figs. 4b,
295 4c, 4e). In years of 2013 and 2016, the difference between observed and simulated
296 streamflow is relatively small, and the average difference is 96 m³/s (Figs. 4a, 4d).

297 Figure 5 shows the hourly streamflow simulation results for a few flood events.
298 Figure 5a shows that the CSSPv2 model can accurately simulate the streamflow
299 response to a rainfall event after a dry period. Figures 5b-5d show that for
300 instantaneous heavy rainfall events, the CSSPv2 model over-predicted the water loss
301 during recession period. Figures 5e-5f show that for continuous rainfall events, the
302 simulated streamflow has a larger fluctuation than observation. The simulated
303 streamflow is also smoother than observation. Nevertheless, the NSE for the hourly
304 streamflow simulation is 0.61, which suggests that CSSPv2 has an acceptable
305 performance at hourly time scale.

306 *3.2 Bias correction of TIGGE-ECMWF meteorological forecasts*

307 The resolution of TIGGE-ECMWF grid data is 0.25° , so the data was
308 interpolated to 5km grid to drive the CSSPv2 model. We calculated both observations'
309 and TIGGE-ECMWF's yearly average precipitation and temperature, then performed
310 a bias correction by adding back the difference (for precipitation) or multiplying back
311 the ratio (for temperature) to match the observations' averages. Figure 6 shows the
312 correlation coefficient and RMSE of TIGGE-ECMWF precipitation and temperature

313 forecasts as compared against observations, either before or after bias correction. The
314 51-ensemble mean precipitation and temperature (the red dashed lines) shows better
315 performance than the best ensemble members (the green dashed lines), with an
316 average RMSE reduction of 3.66 mm/day and average correlation increase of 0.04 for
317 precipitation, and average RMSE reduction of 0.1K and average correlation increase
318 of 0.03 for temperature. After bias correction, the 51-ensemble means still perform
319 better than best ensemble members. Compared with ensemble mean results before
320 bias correction, the RMSE reduced by 0.23 mm/day for the bias-corrected
321 precipitation, and reduced by 1K for the bias-corrected surface air temperature. For
322 the bias-corrected ensemble mean results, the average RMSE and correlation are 14.6
323 mm/day and 0.44 for precipitation, and 1.25 K and 0.87 for surface air temperature.

324 *3.3 Comparison between ESP-Hydro and Meteo-Hydro streamflow forecast*

325 Figure 7 presents the variations of RMSE and CRPS for ESP-Hydro and
326 Meteo-Hydro hourly streamflow forecast at Yantan hydrological gauge. For
327 probabilistic forecast, Figure 7a shows that the CRPS for Meteo-Hydro streamflow
328 forecast ranges from 165 to 225 m³/s while the CRPS for ESP-Hydro streamflow
329 forecast ranges from 170 to 230 m³/s. The Meteo-Hydro approach performs better
330 than ESP-Hydro with lower CRPS at all lead times, with an average of 6%
331 improvement in CRPSS (Figure 7c). For deterministic forecast, Figure 7b shows that
332 the RMSE for Meteo-Hydro streamflow forecast ranges from 250 to 350 m³/s, while
333 the RMSE for ESP-Hydro streamflow forecast ranges from 250 to 390 m³/s. The
334 Meteo-Hydro approach also performs better than ESP-Hydro with lower RMSE at all

335 lead times especially after 3 days, with the average reduction of RMSE reaching 6%
336 (Figure 7d).

337 Figure 7 also shows that both forecast skills have a similar diurnal cycle, where
338 RMSE and CRPS reach their peaks around 00UTC and drop to their lows at 06UTC.
339 Figure 8 shows the diurnal cycle of model employed variables, which are observed
340 catchment mean rainfall, observed streamflow at Yantan and Longtan hydrological
341 gauges, to explain the diurnal cycle of ESP-Hydro and Meteo-Hydro forecasting skills.
342 These three input variables show different diurnal patterns. The observed rainfall
343 starts to rise at 00UTC and reaches its maximum at 06UTC. The observed streamflow
344 at Yantan hydrological gauge drops to its minimum at 12UTC and rises to its
345 maximum at 00UTC. The streamflow from upstream Longtan hydrological gauge
346 starts to drop at 00UTC and reaches its minimum at 06UTC. After comparing these
347 diurnal cycles with the cycle of forecast skill, it is found that the forecast skill
348 decreases when the upstream Longtan outflow starts to decrease, and the precipitation
349 starts to increase. When the upstream Longtan outflow increases and the precipitation
350 starts to decrease (after 06UTC), the forecast skill rises. Such information indicates
351 that the hydrological model performs worse in the case of heavier rainfall event, and
352 the decrease of upstream outflow may amplify such degradation when the portion of
353 interval rainfall-runoff increased.

354 *3.4 Meteo-Hydro-LSTM streamflow forecast*

355 Machine learning methods can recognize patterns hidden in input data and can
356 simulate or predict streamflow without explicit descriptions of the underlying physical

357 processes. Figure 9 shows the RMSE of Meteo-Hydro-LSTM streamflow forecast
358 using the ensemble mean hydrological forecast as described in the section above, and
359 the past 6-hour observed streamflow of Yantan hydrological gauge as input.
360 Compared with Meteo-Hydro and ESP-Hydro approach, applying LSTM model can
361 further decrease the RMSE within the first 72 hours. The RMSE of
362 Meteo-Hydro-LSTM approach ranges from 205 to 363 m³/s during these three days,
363 suggesting an average of 6% improvement against Meteo-Hydro approach.

364 Figure 9 also shows the RMSE of LSTM streamflow forecast only using the past
365 6-hour observed streamflow of Yantan hydrological gauge as input. Without using the
366 physical model forecast, RMSE is improved only when the lead time is less than 1 day.
367 And the performance of LSTM is far worse than Meteo-Hydro streamflow forecast
368 when lead time is more than 2 days.

369 Figure 10 shows several examples of streamflow forecasts by
370 Meteo-Hydro-LSTM approach and Meteo-Hydro approaches to show the forecast
371 improvements in details. The Meteo-Hydro-LSTM approach reduced the flood peak
372 value and the water loss during flood recession period compared with Meteo-Hydro
373 streamflow forecast approach, which improves the streamflow prediction for most
374 cases (Figs. 10b-10f). However, when the upstream reservoir's flood operation is
375 triggered by continuous heavy rain, the Meteo-Hydro may underpredict the
376 streamflow. With the LSTM model further decreases the streamflow, the
377 Meteo-Hydro-LSTM method can end up with worsening the streamflow forecast,

378 which means the machine learning method may improve forecasts when trained in
379 different flood operating situations (Figure 10a).

380 **4. Conclusions**

381 In this study, we developed and evaluated a streamflow forecasting framework
382 by coupling meteorological forecasts with a land surface hydrological model (CSSPv2)
383 and a machine learning method (LSTM) over a cascade reservoir catchment using
384 hindcast data from 2013 to 2017. The monthly observed runoff was used to calibrate
385 the runoff generation module of the CSSPv2 model grid by grid, and the hourly
386 observed streamflow at Yantan hydrological gauge was used to calibrate the routing
387 module of the CSSPv2 model. Then, the bias-corrected TIGGE-ECMWF ensemble
388 forecasts were used to drive the CSSPv2 for streamflow forecasts, and the LSTM
389 model was used to correct the streamflow forecasts, resulted in an integrated
390 meteorological-hydrological-machine learning forecast framework.

391 With automatic offline calibration of the CSSPv2 model, and the NSE values are
392 0.96, 0.92 and 0.61 for streamflow simulations at the Yantan gauge at monthly, daily
393 and hourly time scales, respectively. The bias-corrected ensemble mean
394 TIGGE-ECMWF forcings which perform the best among all ensemble members,
395 show average RMSE and correlation of 14.6 mm/day and a 0.44 for precipitation
396 forecasts, and 1.3 K and 0.87 for surface air temperature forecasts. By comparing with
397 the hourly observed streamflow, the integrated hydrometeorological forecast approach

398 (Meteo-Hydro) increases the probabilistic and deterministic forecast skill against the
399 initial condition-based approach (ESP-Hydro) by 6%.

400 Adding LSTM model to the hydrometeorological forecast (Meteo-Hydro-LSTM)
401 can further reduce the forecast error. Within the first 72 hours, LSTM can improve the
402 forecast skill with a maximum of 25% and an average of 6%. However, if we do not
403 use the streamflow predicted by Meteo-Hydro, the error from the LSTM increases
404 rapidly after 24 hours, and the historical data-based LSTM method performs worse
405 than the Meteo-Hydro method. Most cascade reservoirs yet cannot forecast
406 streamflow beyond 6 hours, and the integrated Meteo-Hydro-LSTM approach has
407 potential to improve the forecasts at long leads. This study mainly focused on
408 exploring the added values of meteorology-hydrology coupled forecast and LSTM
409 forecast in a non-closed catchment, so the forecast uncertainty from upstream outflow
410 was ignored by using the observed outflow. In the future, the upstream outflow
411 forecast is planned to include, but this requires the development of upstream
412 hydrometeorological forecast capability, as well as the reservoir regulation forecast
413 that is very challenging. The artificial intelligence (AI) techniques are expected to
414 complement the physical model for reservoir regulation forecast.

415

416 **Acknowledgement.** This work was supported by National Key R&D Program of
417 China (2018YFA0606002), National Natural Science Foundation of China
418 (41875105), and Natural Science Foundation of Jiangsu Province for Distinguished
419 Young Scholars (BK20211540).

420

421 **Data availability.** The TIGGE-ECMWF hindcast data can be downloaded from
422 <https://apps.ecmwf.int/datasets/data/tigge/levtype=sfc/type=pf/> (Parsons et al., 2017),
423 the in-situ observations and simulation data are available upon request.

424

425 **References**

- 426 Abrahart, R. J., Anctil, F., Coulibaly, P., Dawson, C. W., Mount, N. J., See, L. M., et
427 al.: Two decades of anarchy? emerging themes and outstanding challenges for
428 neural network river forecasting. *Prog. Phys. Geogr.* 36(4), 480-513.
429 <https://doi.org/10.1177/0309133312444943>, 2012.
- 430 Adnan, R.M., et al.: Daily streamflow prediction using optimally pruned extreme
431 learning machine. *J. Hydrol.* 577. <https://doi.org/10.1016/j.jhydrol.2019.123981>,
432 2019.
- 433 Alfieri, L., Burek, P., Dutra, E., Krzeminski, B., & Pappenberger, F.: GloFAS-global
434 ensemble streamflow forecasting and flood early warning. *Hydrol. Earth Syst.*
435 *Sci.* 17 (3), 1161–1175. <https://doi.org/10.5194/hess17-1161-2013>, 2013.
- 436 Balint, G., Csik, A., Bartha, P., Gauzer, B., Bonta, I.: Application of meteorological
437 ensembles for Danube flood forecasting and warning. In: Marsalek, J., Stancalie,
438 G., Balint, G. (Eds.), *Transboundary Floods: Reducing Risks through Flood*
439 *Management*. Springer, NATO Science Series, Dordrecht, The Netherlands, pp.
440 57–68. https://doi.org/10.1007/1-4020-4902-1_6, 2006.
- 441 Bougeault, P., et al.: The THORPEX interactive grand global ensemble, *Bull. Am.*
442 *Meteorol. Soc.*, 91, 1059–1072. <http://dx.doi.org/10.1175/2010BAMS2853.1>,
443 2010.
- 444 Dai, Y., Dickinson, R. E., Wang, Y. P.: A two-big-leaf model for canopy temperature,
445 photosynthesis, and stomatal conductance. *J. Clim.* 17(12),2281–2299.
446 [https://doi.org/10.1175/1520-0442\(2004\)017<2281:ATMFCT>2.0.CO;2](https://doi.org/10.1175/1520-0442(2004)017<2281:ATMFCT>2.0.CO;2), 2004.

447 Dai, Y., Zeng, X., Dickinson, R. E., Baker, I., Bonan, G. B., Bosilovich, M. G., et al.:
448 The Common Land Model. *Bull. Am. Meteorol. Soc.* 84(8), 1013–1024.
449 <https://doi.org/10.1175/BAMS-84-8-1013>, 2003.

450 Dang, T. D., Chowdhury, A. K., Galelli, S.: On the representation of water reservoir
451 storage and operations in large-scale hydrological models: implications on
452 model parameterization and climate change impact assessments. *Hydrol. Earth
453 Syst. Sci.*, 24, 397–416. <https://doi.org/10.5194/hess-24-397-2020>, 2020.

454 Day, G.N.: Extended Streamflow Forecasting Using NWSRFS. *J. Water Resour. Plan
455 Manag.* 111 (2): 157-170, 1985.

456 Duan, Q., Sorooshian, S., Gupta, V. K.: Optimal use of SCEUA global optimization
457 method for calibrating watershed models, *J. Hydrol.*, 158, 265–284,
458 [https://doi.org/10.1016/0022-1694\(94\)90057-4](https://doi.org/10.1016/0022-1694(94)90057-4), 1994.

459 Gao, X., Zeng, Y., Wang, J., Liu, H.: Immediate impacts of the second impoundment
460 on fish communities in the Three Gorges Reservoir, *Environ. Biol. Fish.*, 87,
461 163–173. <https://doi.org/10.1007/s10641-009-9577-1>, 2010.

462 Getirana, A. C. V., Boone, A., Yamazaki, D., Decharme, B., Papa, F., and Mognard, N.:
463 The Hydrological Modeling and Analysis Platform (HyMAP): Evaluation in the
464 Amazon Basin, *J. Hydrometeorol.*, 13, 1641–1665,
465 <https://doi.org/10.1175/JHM-D-12-021.1>, 2012.

466 Graaf, I. D., Sutanudjaja, E. H., Beek, L. V., et al.: A high-resolution global-scale
467 groundwater model. *Hydrol. Earth Syst. Sci.* 19(2):823-837.
468 <https://doi.org/10.5194/hess-19-823-2015>, 2015.

469 Hao, Z., Aghakouchak, A., Phillips, T. J.: Changes in concurrent monthly precipitation
470 and temperature extremes. *Environ. Res. Lett.* 8(3), 1402-1416.
471 <https://doi.org/10.1088/1748-9326/8/3/034014>, 2013.

472 Hopson, T., Webster, P.: A 1–10 day ensemble forecasting scheme for the major river
473 basins of Bangladesh: forecasting severe floods of 2003–2007. *J. Hydrometeorol.*
474 11(3), 618-641. <https://doi.org/10.1175/2009JHM1006.1>, 2010.

475 Hornberger, G. M., E. W. Boyer.: Recent advances in watershed modeling, U.S. Natl.
476 Rep. Int. Union Geod. Geophys. 1991 – 1994, *Rev. Geophys.*, 33, 949 – 957.
477 <https://doi.org/10.1029/95RG00288>, 1995.

478 Humphrey, G.B., Gibbs, M.S., Dandy, G.C., Maier, H.R.: A hybrid approach to
479 monthly streamflow forecasting: Integrating hydrological model outputs into a
480 Bayesian artificial neural network. *J. Hydrol.* 540, 623–640.
481 <https://doi.org/10.1016/j.jhydrol.2016.06.026>, 2016.

482 Jasper, K., Gurtz, J., Lang, H.: Advanced flood forecasting in Alpine watersheds by
483 coupling meteorological observations and forecasts with a distributed
484 hydrological model. *J. Hydrol.* 267 (1–2), 40–52.
485 [https://doi.org/10.1016/S0022-1694\(02\)00138-5](https://doi.org/10.1016/S0022-1694(02)00138-5), 2002.

486 Jaun, S., Ahrens, B., Walser, A., Ewen, T., Schär, C.: A probabilistic view on
487 the August 2005 floods in the upper Rhine catchment. *Nat. Hazard Earth Sys.* 8,
488 281–291. <https://doi.org/10.5194/nhess-8-281-2008>, 2008.

489 Ji, P., X. Yuan., Y. Jiao., C. Wang., S. Han., C. Shi.: Anthropogenic contributions to
490 the 2018 extreme flooding over the upper Yellow River basin in China. *Bull. Am.*

491 Meteorol. Soc. 101(1), S89-S94, <https://doi.org/10.1175/BAMS-D-19-0105.1>,
492 2020.

493 Kirchner, J. W.: Getting the right answers for the right reasons: Linking measurements,
494 analyses, and models to advance the science of hydrology, *Water Resour. Res.*
495 42, 1–5. <https://doi.org/10.1029/2005WR004362>, 2006.

496 Kisi, O.: Streamflow forecasting using different artificial neural network algorithms. *J.*
497 *Hydrol. Eng.* 12 (5), 532–539.
498 [https://doi.org/10.1061/\(ASCE\)1084-0699\(2007\)12:5\(532\)](https://doi.org/10.1061/(ASCE)1084-0699(2007)12:5(532)), 2007.

499 Kollet, S. J., Maxwell, R. M., Woodward, C. S., Smith, S., Vanderborght, J., &
500 Vereecken, H., et al.: Proof of concept of regional scale hydrologic simulations
501 at hydrologic resolution utilizing massively parallel computer resources. *Water*
502 *Resour. Res.* 46(4). <https://doi.org/10.1029/2009WR008730>, 2010.

503 Kratzert, F., Klotz, D., Brenner, C., Schulz, K., Herrnegger, M.: Rainfall–runoff
504 modelling using long short-term memory (LSTM) networks. *Hydrol. Earth Syst.*
505 *Sci.* 22 (11), 6005–6022. <https://doi.org/10.5194/hess-22-6005-2018>, 2018.

506 Kratzert, F., Klotz, D., Herrnegger, M., Sampson, A. K., Hochreiter, S., Nearing, G. S.:
507 Towards Improved Predictions in Ungauged Basins: Exploiting the Power of
508 Machine Learning. *Water Resour. Res.* 55.
509 <https://doi.org/10.1029/2019wr026065>, 2019.

510 Leith, C. E.: Theoretical skill of monte carlo forecasts. *Mon. Weather Rev.* 102(6),
511 409-418. [https://doi.org/10.1175/1520-0493\(1974\)102:2.0.CO;2](https://doi.org/10.1175/1520-0493(1974)102:2.0.CO;2), 1974.

512 Luo, X., Li, H. Y., Ruby, L. L., Tesfa, T. K., Augusto, G., & Fabrice, P., et al.:

513 Modeling surface water dynamics in the amazon basin using mosart-inundation
514 v1.0: impacts of geomorphological parameters and river flow representation.
515 Geosci. Model. Dev., 10(3), 1-42. <https://doi.org/10.5194/gmd-10-1233-2017> ,
516 2017.

517 Mulvaney, T. J.: On the use of self-registering rain and flood gauges in making
518 observations of the relations of rainfall and of flood discharges in a given
519 catchment, in: Proceedings Institution of Civil Engineers, Dublin, Vol. 4, 18–31,
520 1850.

521 Pappenberger, F., Ramos, M. H., Cloke, H. L., Wetterhall, F., Alfieri, L., Bogner, K.,
522 et al.: How do I know if my forecasts are better? Using benchmarks in
523 hydrological ensemble prediction. J. Hydrol. 522, 697–713.
524 <https://doi.org/10.1016/j.jhydrol.2015.01.024>, 2015.

525 Parsons, D. B., Beland, M., Burridge, D., Bougeault, P., Brunet, G., Caughey, J., et al.:
526 Thorpex research and the science of prediction. Bull. Am. Meteorol. Soc., 98,
527 807-830, <https://doi.org/10.1175/BAMS-D-14-00025.1> , 2017.

528 Robertson, D. E., Wang, Q. J.: Seasonal Forecasts of Unregulated Inflows into the
529 Murray River, Australia. Water. Resour. Manag. 27(8):2747–2769.
530 <https://doi.org/10.1007/s11269-013-0313-4>, 2013.

531 Shao, J., Wang, J., Lv, S., Bing, J.: Spatial and temporal variability of seasonal
532 precipitation in Poyang Lake basin and possible links with climate indices.
533 Hydrol. Res. 47(S1):51–68. <https://doi.org/10.2166/nh.2016.249>, 2016.

534 Toth, Z., Zhu, Y., Marchok, T.: The use of ensembles to identify forecasts with small

535 and large uncertainty. *Weather Forecast* 16(4), 463-463.
536 [https://doi.org/10.1175/1520-0434\(2001\)0162.0.CO;2](https://doi.org/10.1175/1520-0434(2001)0162.0.CO;2), 2001.

537 Wang, R., Zhang, J., Guo, E., Zhao, C., Cao, T.: Spatial and temporal variations of
538 precipitation concentration and their relationships with large-scale atmospheric
539 circulations across Northeast China. *Atmos. Res.* 222:62–73.
540 <https://doi.org/10.1016/j.atmosres.2019.02.008>, 2019.

541 Wilks, D. S.: *Statistical Methods in the Atmospheric Sciences*, Volume 91, Second
542 Edition (International Geophysics), 2005.

543 Wood, E. F., et al.: Hyperresolution global land surface modeling: Meeting a grand
544 challenge for monitoring Earth’s terrestrial water. *Water Resour. Res.*, 47,
545 W05301, <https://doi.org/10.1029/2010WR010090>, 2011.

546 Xu, Y.P., Gao, X., Zhang, Y., Kang, L.: Coupling a regional climate model and
547 distributed hydrological model to assess future water resources in Jinhua River
548 Basin, East China. *ASCE. J. Hydrol. Eng.* 20, 2015,
549 [https://doi.org/10.1061/\(ASCE\) HE.1943-5584.0001007](https://doi.org/10.1061/(ASCE) HE.1943-5584.0001007), 2015.

550 Yang, S., Yang, D., Chen, J., Santisirisomboon, J., Zhao, B.: A physical process and
551 machine learning combined hydrological model for daily streamflow
552 simulations of large watersheds with limited observation data. *J. Hydrol.* 590,
553 125206. <https://doi.org/10.1016/j.jhydrol.2020.125206>, 2020.

554 Yaseen, Z.M., Sulaiman, S.O., Deo, R.C., Chau, K.-W.: An enhanced extreme learning
555 machine model for river flow forecasting: State-of-the-art, practical applications
556 in water resource engineering area and future research direction. *J. Hydrol.* 569,

557 387–408. <https://doi.org/10.1016/j.jhydrol.2018.11.069>, 2018.

558 Ye, A., Duan, Q., Yuan, X., Wood, E. F., Schaake, J.: Hydrologic post-processing of
559 MOPEX streamflow simulations. *J. Hydrol.* 508, 147-156,
560 doi:10.1016/j.jhydrol.2013.10.055, 2014

561 Yuan, X., Ma, F., Wang, L., Zheng, Z., Ma, Z., Ye A., Peng, S.: An experimental
562 seasonal hydrological forecasting system over the Yellow River basin-Part 1:
563 Understanding the role of initial hydrological conditions. *Hydrol. Earth Syst. Sci.*
564 20, 2437–2451, <https://doi.org/10.5194/hess-20-2437-2016>, 2016.

565 Yuan, X., S. Wang, and Z.-Z. Hu, 2018a: Do climate change and El Niño increase
566 likelihood of Yangtze River extreme rainfall? *Bull. Am. Meteorol. Soc.* 99,
567 S113-S117, <https://doi.org/10.1175/BAMS-D-17-0089.1>, 2018a.

568 Yuan, X., Ji, P., Wang, L., Liang, X. Z., Yang, K., Ye, A., et al.: High - resolution land
569 surface modeling of hydrological changes over the sanjiangyuan region in the
570 eastern tibetan plateau: 1. model development and evaluation. *J. Adv. Model*
571 *Earth Syst.* <https://doi.org/10.1029/2018MS001412>, 2018b.

572 Zhang, Y., Erkyihum, S. T., Block, P.: Filling the GERD: evaluating hydroclimatic
573 variability and impoundment strategies for Blue Nile riparian countries, *Water*
574 *Int.*, 41, 593–610. <https://doi.org/10.1080/02508060.2016.1178467>, 2016.

575 Zhao, T.T.G., Cai, X.M., Yang, D.W.: Effect of streamflow forecast uncertainty on
576 real-time reservoir operation. *Adv. Water Resour.* 34 (4), 495–504,
577 <https://doi.org/10.1016/j.advwatres.2011.01.004>, 2011.

578 Zhu, E., X. Yuan., A. Wood.: Benchmark Decadal Forecast Skill for Terrestrial Water

579 Storage Estimated by an Elasticity Framework. Nat. Commun. 10, 1237,

580 <https://doi.org/10.1038/s41467-019-09245-3>, 2019.

581

582 **Table 1.** Information of hydrological gauges.

| Gauge | Longitude ($^{\circ}$ E) | Latitude ($^{\circ}$ N) | Drainage area (km^2) |
|----------|------------------------------|-----------------------------|------------------------------------|
| Longtan | 107.09 | 25.00 | - |
| Yantan | 107.50 | 24.11 | 5950 (orange area in Fig. 1) |
| Luofu | 107.36 | 24.90 | 800 (green area in Fig. 1) |
| Jiazhuan | 107.12 | 24.21 | 2150 (purple area in Fig. 1) |

583

584 **Table 2.** Information of hydrological datasets

| Dataset | Time Range | Time step |
|----------------------------------|-----------------------|-----------|
| Rain Gauge Observation Forcing | 2013/1/1 ~ 2017/12/31 | Hourly |
| Longtan & Yantan Discharge Gauge | 2013/1/1 ~ 2017/12/31 | Hourly |
| Streamflow data | | |
| Jiazhuan & Luofu Discharge Gauge | 2013/4/1 ~ 2017/9/30 | Daily |
| Streamflow data | | |
| TIGGE-ECMWF Forecast Forcing | 2013/4/1 ~ 2017/9/30 | Hourly |

585

586 **Table 3.** Descriptions of calibrated parameters

| Parameters | Range |
|---|-----------------------|
| Maximum velocity of baseflow (mm/day) | 0.00000116 ~ 0.000579 |
| Fraction of maximum velocity of baseflow where non-linear baseflow begins | 0.001 ~ 0.99 |
| Fraction of maximum soil moisture where non-linear baseflow occurs | 0.2 ~ 0.99 |
| Variable infiltration curve parameter | 0.001 ~ 1 |
| River width (m) | 0 ~ 101.16 |
| River depth (m) | 0 ~ 6.46 |
| River density (km/km ²) | 0.049 ~ 1.03 |
| River roughness | 0.033 ~ 0.05 |
| River slope | 0.015 ~ 0.47 |

587

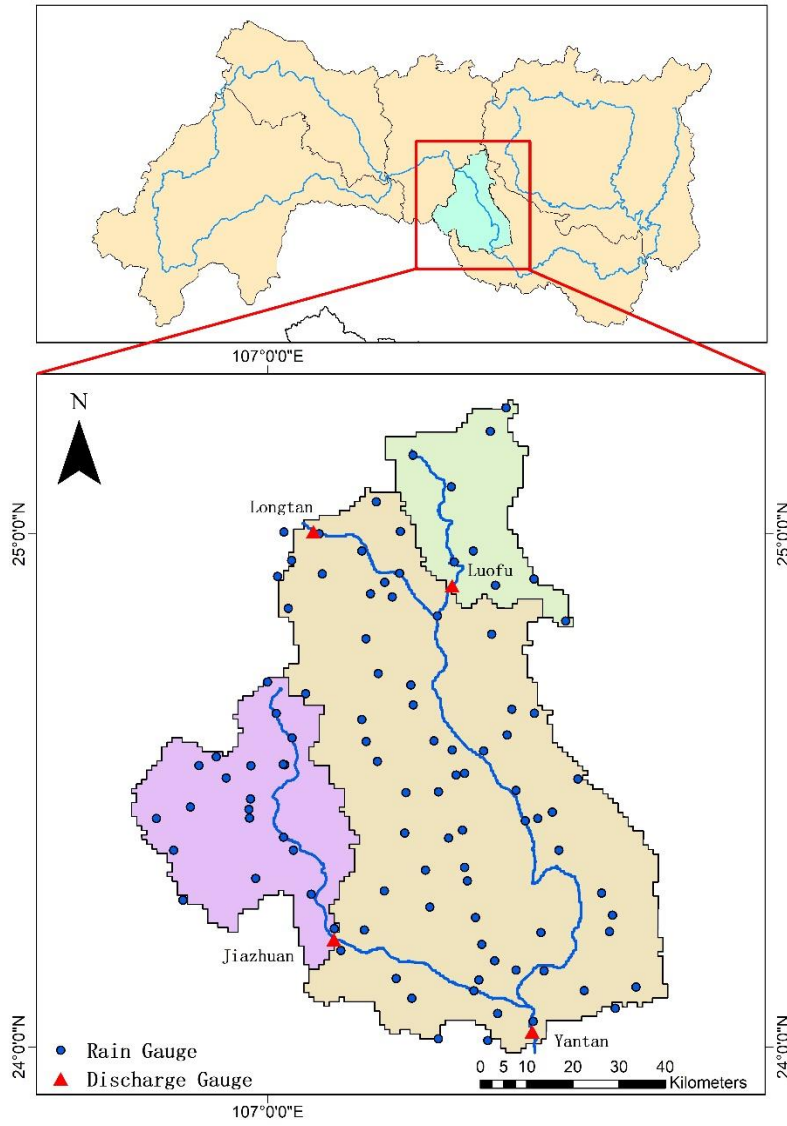
588 **Table 4.** Experimental design in this study.

| Experiments | Description |
|------------------|--|
| ESP-Hydro | Using CSSPv2 land surface hydrological model driven by randomly-sampled historical meteorological forcings |
| Meteo-Hydro | Using CSSPv2 model driven by bias-corrected TIGGE-ECMWF hindcast meteorological forcings |
| Meteo-Hydro-LSTM | Using LSTM model to correct streamflow from Meteo-Hydro hindcast |
| LSTM | Using LSTM model to forecast streamflow based on observation only |

589

590

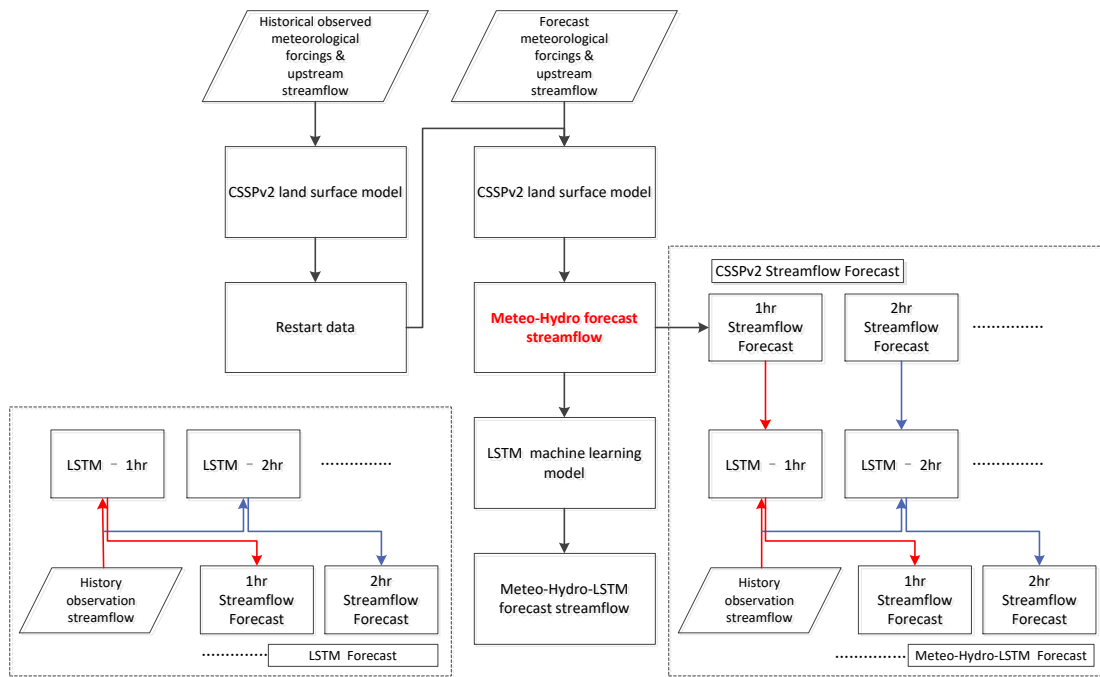
591



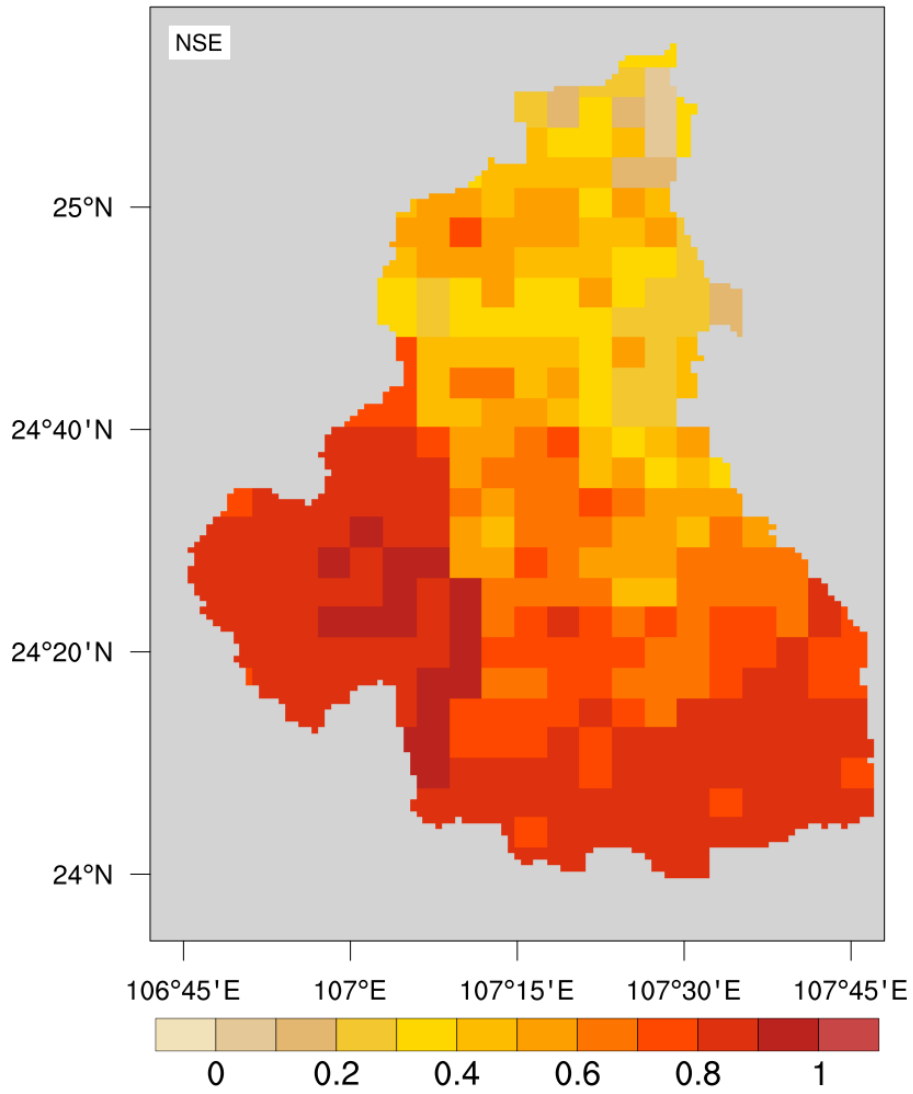
592

593 **Figure 1.** Locations of discharge gauges and rain gauges over the Yantan basin.

594

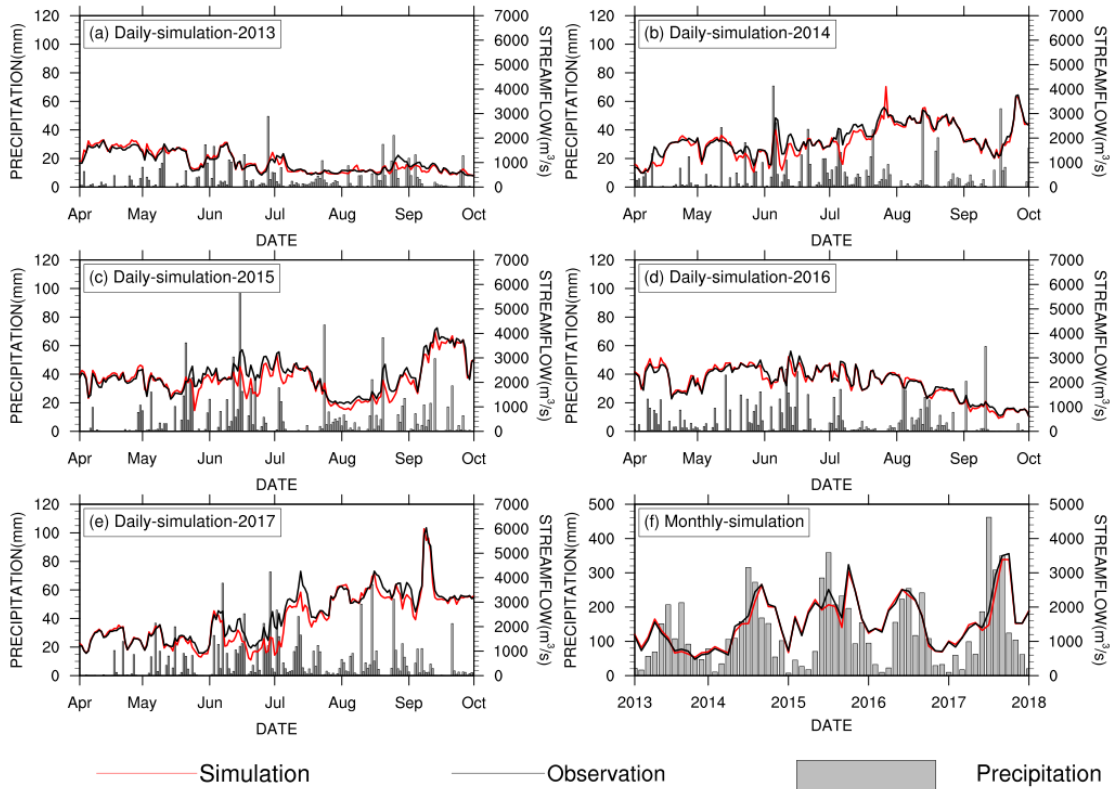


596 **Figure 2.** A diagram for the integrated hydrometeorological and machine learning
597 streamflow prediction.



600 **Figure 3.** Nash-Sutcliff efficiency coefficients for the calibrated grid runoff simulation

601 from CSSPv2.

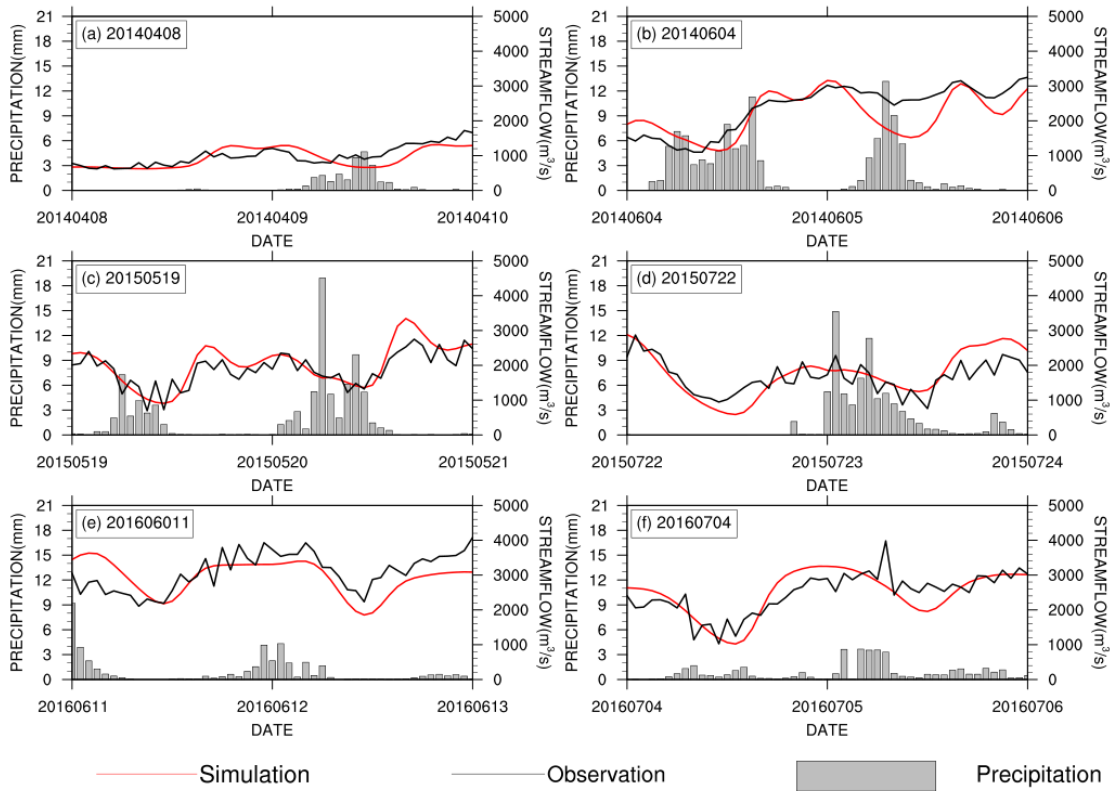


603

604 **Figure 4.** Evaluation of streamflow simulations at Yantan gauge. The black and red

605 lines are observed and simulated streamflow. (a)-(e) are for daily streamflow, and (f)

606 is for monthly streamflow. The gray bars represent daily (or monthly) precipitation.



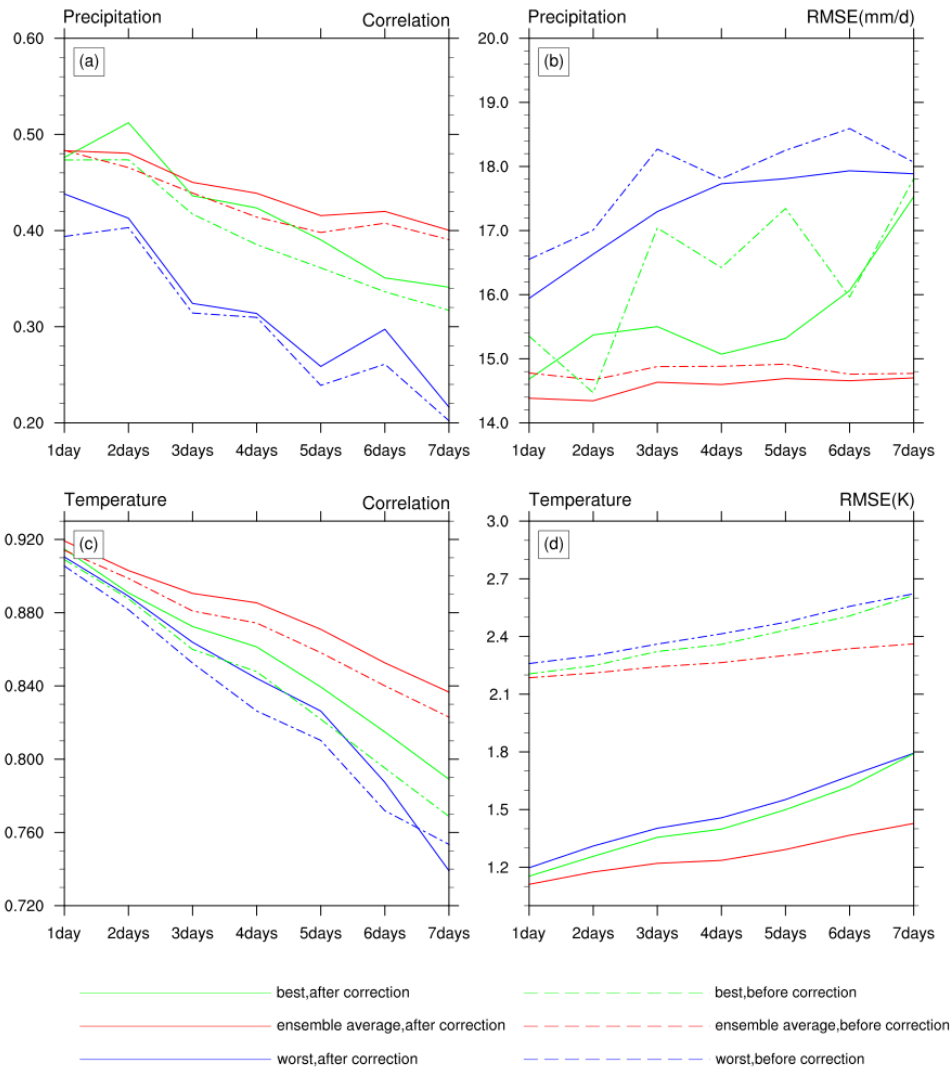
608

609 **Figure 5.** The same as Figure 4, but for the evaluation of hourly streamflow

610 simulations at Yantan gauge.

611

612

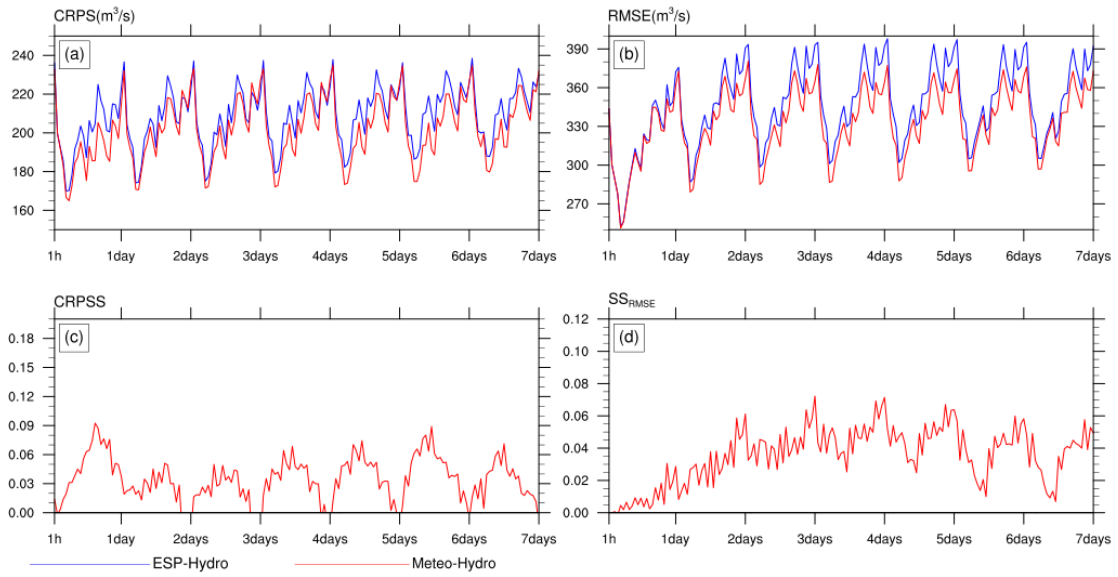


613

614 **Figure 6.** Evaluation of precipitation and temperature hindcasts from
615 TIGGE-ECMWF. The red and blue lines represent the best and worst results among 51
616 TIGGE-ECMWF ensemble members respectively, and the green lines represent the
617 results for the ensemble means of 51 members. Solid and dashed lines represent the
618 results after and before bias corrections, respectively.

619

620

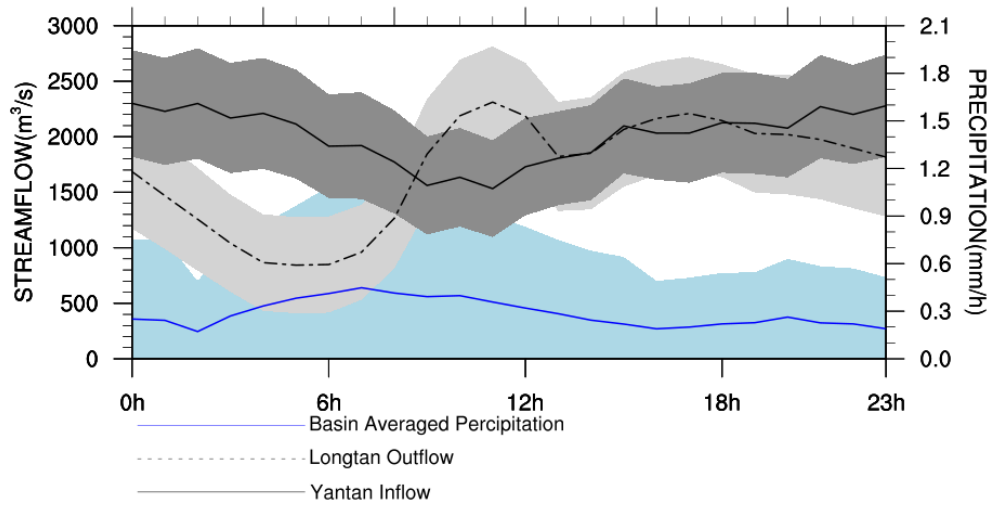


621

622 **Figure 7.** (a) Continuous Ranked Probability Score (CRPS) and (b) Root Mean
623 Squared Error (RMSE) for daily streamflow ensemble forecasts at Yantan gauge. (c)
624 and (d) are the skill score in terms of CRPS and RMSE for Meteo+Hydro, where
625 ESP+Hydro is used as reference forecast.

626

627



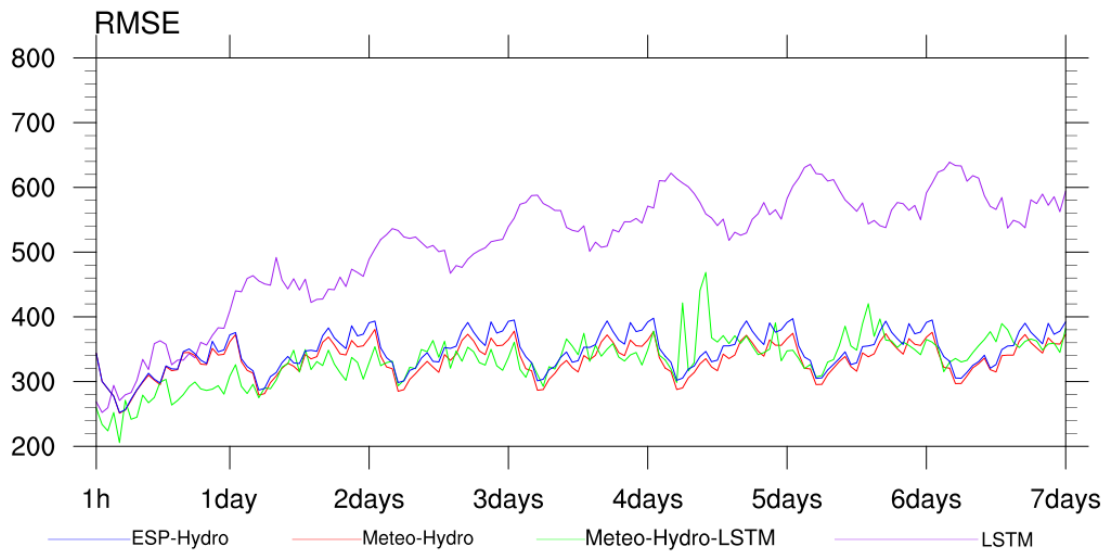
628

629 **Figure 8.** Diurnal cycle of Longtan outflow (m^3/s ; dashed black line), Yantan inflow

630 (m^3/s ; solid black line) and basin-averaged precipitation (mm/h ; blue line), as well as

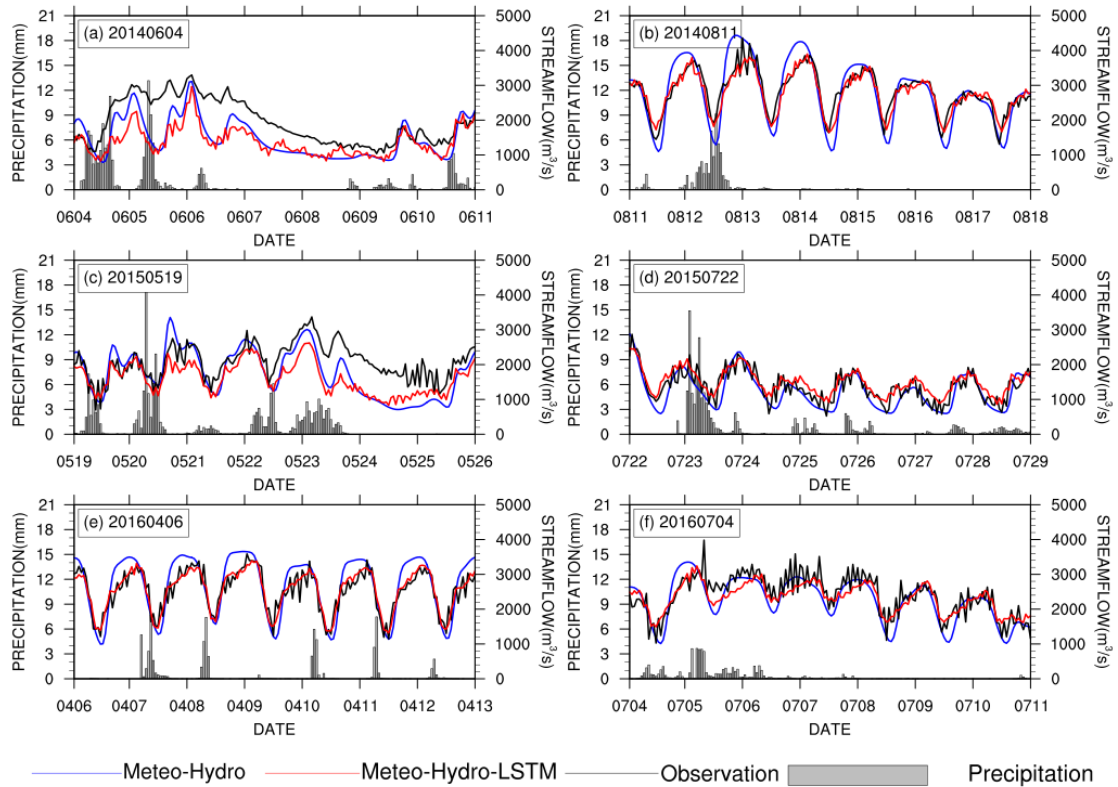
631 their ranges. The time shown in this figure is universal time.

632



633

634 **Figure 9.** RMSE (m^3/s) for hourly streamflow hindcasts from four forecast
635 approaches. The green line represents the Meteo+Hydro+LSTM forecast, the red line
636 represents the Meteo+Hydro forecast, the blue line represent the ESP+Hydro forecast,
637 and the purple line represents the LSTM forecast based on historical streamflow
638 observation alone.



639

640 **Figure 10.** Evaluation of the forecast approaches for a few flooding events. The black
 641 lines are observed streamflow from Yantan hydrological gauge, the blue lines are the
 642 Meteo+Hydro ensemble mean streamflow forecast, and the red lines are the
 643 Meteo+Hydro+LSTM forecast streamflow by using Meteo+Hydro ensemble mean
 644 forecast with LSTM. The gray bars represent hourly precipitation averaged over the
 645 basin.